UC Riverside
2019 Publications

Title

An Experimental and Modeling Study of Nanoparticle Formation and Growth from Dimethylamine and Nitric Acid

Permalink

Journal

ISSN

Authors

Chee, Sabrina
Myllys, Nanna
Barsanti, Kelley C
et al.

Publication Date

DOI

Peer reviewed

An Experimental and Modeling Study of Nanoparticle Formation and Growth from Dimethylamine and Nitric Acid

Sabrina Chee,[†] Nanna Myllys,[†] Kelley C. Barsanti,[‡,§] Bryan M. Wong,[‡,∥] and James N. Smith*[†]

[†]Department of Chemistry, University of California, Irvine, California 92617, United States

[‡]Department of Chemical & Environmental Engineering, [§]Center for Environmental Research and Technology, and [∥]Materials Science & Engineering Program, University of California, Riverside, California 92521, United States

Ⓢ *Supporting Information*

ABSTRACT: The size-resolved composition of nanoparticles formed and grown through acid−base reactive uptake has been studied in the laboratory by reacting gas-phase nitric acid (HNO_3) and dimethylamine (DMA) in a flow tube under dry (<5% RH) and humid (∼55% RH) conditions. Size-resolved nanoparticle composition was measured by a thermal desorption chemical ionization mass spectrometer over the diameter range of 9−30 nm. The nanoparticle geometric mean diameter grew in the presence of water compared to dry conditions. Acid/base ratios of HNO_3-DMA particles at all measured sizes did not strongly deviate from neutral (1:1) in either RH condition, which contrasts with prior laboratory studies of nanoparticles made from sulfuric acid (H_2SO_4) and base. Theoretical methods were used to investigate the underlying chemical processes that explain observed differences in the compositions of HNO_3-DMA and H_2SO_4-DMA particles. Calculations of HNO_3-DMA cluster stability indicated that a 1:1 acid/base ratio has >10^7 smaller evaporation rates than any other acid/base ratio in this system, and measured nanoparticle composition confirm this to be the most stable pathway for growth up to 30 nm particles. This study demonstrates that nanoparticle formation and growth via acid−base reactive uptake of HNO_3 and DMA follow the thermodynamic theory, likely because of both components' volatility.
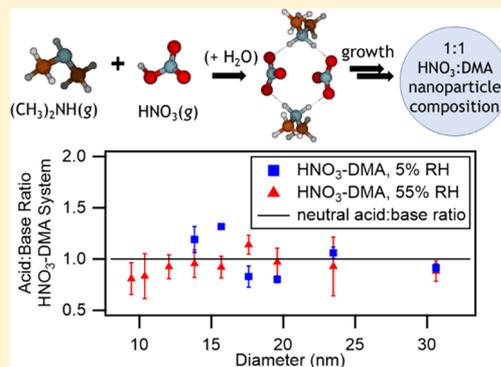
■ INTRODUCTION

New particle formation (NPF) events are large contributors to the global population of cloud condensation nuclei,[1,2] which can affect climate and precipitation by influencing cloud formation. However, the growth processes for nanoparticles (<100 nm in diameter) formed from these NPF events are not well understood.[2] At these sizes, the Kelvin effect reduces the number of gases that can contribute to nanoparticle growth by condensation.[3] Sulfuric acid is the most studied contributor to nanoparticle growth[4−13] because of its extremely low volatility and high acidity; however, it has been observed that concentrations of sulfuric acid alone cannot explain all nanoparticle formation and growth.[10,12,14] Measurements of nanoparticle composition at several field studies support this observation where organic species, nitrate, and aminium ions have been detected in coexistence with sulfate in nanoparticles.[15−17]

Acid−base chemistry as a mechanism of reactive uptake into particles, while conceptually simple,[18] is still poorly understood when applied to the formation and growth of clusters and nanoparticles. Clusters of sulfuric acid and ammonia/amines have been measured and have been observed to grow stepwise with sulfuric acid adding first, followed by the addition of base.[12,19,20] This neutralization process implies either a 1:1 or 1:2 acid/base ratio for particles growing via acid−base reactive

uptake. Recently, however, several studies have reported that particles composed of sulfuric acid and base have been observed to be more acidic in particle diameters smaller than 15 nm,[21,22] and in the specific case of H_2SO_4-DMA particles, they even become more basic under dry conditions at some sizes.[23] This disparity between the composition of clusters and nanoparticles in such acid−base systems warrants additional investigation. These prior studies examined trends in nanoparticle composition from reactions of bases with sulfuric acid, a low-volatility diprotic acid. This study supplements these observations with experiments and modeling of reactions of these bases with a monoprotic acid with volatility 5 orders of magnitude higher than sulfuric acid.

Nitric acid (HNO_3) is ubiquitous throughout the atmosphere and is typically present in low ppb$_v$ concentrations.[24−26] Nitrate (NO_3^-) has been observed to be present in atmospheric particles smaller than 50 nm in diameter[15,17] as well as in micrometer-sized particles.[27,28] Typically, nitrate present in particles larger than 100 nm in diameter has been attributed to salt formation of primarily ammonium nitrate and in marine areas sodium nitrate.[3] However, experimental studies
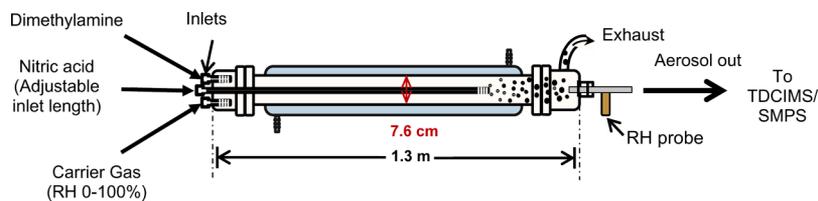
Figure 1. Particle generation flow tube setup.

have shown that ammonium nitrate salts are too volatile to be present in particles smaller than ~50 nm in diameter.[29] It has been suggested that, for these ambient particles in which the Kelvin effect is strong, the detected nitrates are associated with strong bases like amines.[29]

Amines have been observed both in laboratory studies and in ambient air to contribute to nanoparticle growth.[13,30−34] Dimethylamine (DMA) has been measured in particles down to the critical cluster size and is found to stabilize cluster formation with sulfuric acid (H_2SO_4) molecules via salt formation.[19,35,36] However, only a few studies have investigated how nitric acid and amines may form salts to contribute to particle growth in the atmosphere.[31,37,38]

This study focuses on the composition and growth of dimethylaminium nitrate (HNO_3-DMA) nanoparticles from gas-phase reactions of dimethylamine and nitric acid. The observations and theoretical understanding obtained from this study provide insights into the potential role of these compounds in the growth of atmospheric nanoparticles. Additionally, since it has been shown previously that the composition of aerosol particles can be affected by ambient relative humidity,[39] particles were formed under both dry (~5% RH) and humid (~55% RH) conditions, and the corresponding impact on nanoparticle composition was explored. Finally, we supplemented our experimental observations with studies of the initial steps of nitric acid and dimethylamine particle formation with and without the presence of water vapor using theoretical methods.

EXPERIMENTAL AND THEORETICAL METHODS

Particle Generation. The flow tube setup is similar to that used by Chen et al.,[23] except for changes to the nitric acid inlet. Briefly, HNO_3-DMA particles were formed and grown in a 4.8 L flow tube reactor (7.5 cm diameter, 105 cm length) in a temperature-controlled room (Figure 1). Gas-phase nitric acid was introduced to the reactor by flowing N_2 through a 30 cm long saturator containing aqueous nitric acid (Macron Fine Chemicals, aqueous 70%, ACS certified) and then serially diluted. The concentration of HNO_3 vapor was estimated by assuming that it achieves its saturation vapor pressure prior to exiting the saturator. The inlet for this study was altered from the Chen et al. study[23] by the addition of a movable, 1/8" OD stainless steel tube inserted into the inlet end of the flow tube (Figure 1). The stainless-steel tube was capped, and the gaseous nitric acid containing N_2 entered the flow tube through slits cut out of the cap to promote mixing. Gas-phase dimethylamine (DMA) was introduced into the flow tube by flowing nitrogen over a permeation tube (VICI AG International) holding liquid DMA (Sigma Aldrich, 99%). The permeation rate of DMA was determined gravimetrically by measurement of mass loss over time, measured once each month for 6 months. DMA was introduced through a separate inlet at the entrance to the flow tube at 100 cm³ min⁻¹, while

100 cm³ min⁻¹ nitric acid was introduced through the moveable injector ~30 cm downstream. Dry or humidified N_2 was used as the carrier gas added at a third inlet. The mixing ratios for nitric acid and dimethylamine after introduction to the flow tube were ~63 ppm and ~10 ppb, respectively. Humidification was carried out by passing N_2 through a heated flask containing nanopure water (>18 MΩ) followed by a temperature-controlled saturator. Relative humidity was monitored by a home-built temperature and humidity sensor located downstream of the flow tube. The residence time of both gases downstream of the nitric acid inlet was ~40 s prior to sampling. Particle measurements were only taken after gases were introduced to the system for 24 h to ensure equilibration of vapors. No significant increase in wall loss of DMA was detected between the dry and humid conditions (Figure S1).

The particle size distribution was measured with a scanning mobility particle sizer (SMPS), which consisted of a nano-differential mobility analyzer (nano-DMA; Model 3085, TSI, Inc.) and a butanol-based mixing condensation particle counter (mCPC; Model 1720, Brechtel Mfg.). The 50% detection efficiency diameter limit for the CPC used was 7.0 nm, as described by the manufacturer. The sheath and excess flows of the nano-DMA were run with mass-flow-controlled (Alicat Scientific) purified zero air (Model 737-13, Aadco Instruments) and a flow-controlled vacuum pump, respectively. Since these flows are not recirculated, particles made from the humid system will dry, and their measured size distribution will be more representative of the particles sampled for chemical composition analysis.

Nanoparticle Composition Measurements. Particles were sampled directly from the flow tube to a Thermal Desorption Chemical Ionization Mass Spectrometer (TDCIMS), which was already described in detail.[22,29,40] Briefly, 2 LPM of aerosol was sampled continuously from the flow tube and into the TDCIMS inlet. Particles were charged by a unipolar charger[41,42] and size-selected by nano-DMA in which the sheath flow was run with zero air to minimize contamination of the TDCIMS inlet by DMA and HNO_3. Monodisperse particles were collected by electrostatic deposition on a Pt filament held at 3500 V. The collection time ranged from 2 to 360 min, depending on particle size, concentration, and collection efficiency. Once sufficient particle mass was collected onto the filament, it traveled up to the ionization region, which was held at 40 °C and flushed continuously with N_2 to prevent contamination from sample air. The filament was resistively heated from 40 to ~600 °C in front of the sampling orifice to the mass spectrometer to thermally desorb particle components. These components were chemically ionized by negative and positive ion mode reagent ions $(H_2O)_nO_2^-$ and $(H_2O)_nH_3O^+$, respectively (n = 1−3), which were generated via a ²¹⁰Po radioactive source that ionizes trace oxygen and water present in a nitrogen flow. The analyte ions were then detected by a quadrupole mass

spectrometer (Extrel Corp.). The thermal desorption process consisted of the following: the wire maintained ambient temperature for 60 s, ramped to ∼600 °C over 180 s, maintained ∼600 °C for 90 s, and then returned to ambient temperature for 60 s. The total desorption cycle was 6.5 min for each collection. Backgrounds for each sample collection were determined by operating the collection/analysis cycle identically except that a high voltage was not applied to the filament during the collection period so that particles were not collected on the filament.

The ion signal was quantified by integrating the difference between collection and background desorption profiles. To improve the signal-to-noise ratio, ion data associated with the desorbed products of DMA and HNO_3 were integrated during the region of highest desorption during analysis, 60−180 s after the start of the analysis cycle (Figure S2). Additionally, to establish signal-to-collected-mass linearity and to ensure that no loss of particulate components occurred during sample collection, 12 nm diameter particle composition was measured after 5, 7.5, 10, 20, and 30 min of collection time (Figure S3). Calculations of the acid/base ratio were performed by integrating the ion intensity of the detected acid ions and then dividing that by the integrated ion intensity of the detected base ions.

The TDCIMS relative sensitivity to ions associated with dimethylamine and nitric acid was calibrated by measuring the composition of atomized particles. A solution of 2 mM 1:1 HNO_3-DMA was made from concentrated nitric acid (Macron Fine Chemicals, aqueous 70%, ACS certified), dimethylamine (Acros Organics, 40 wt % in water), and water (>18 MΩ). This bulk solution was aerosolized using an atomizer (Model 3076, TSI, Inc.), and the resulting droplets were dried with a Nafion dryer (Perma Pure, Inc.) to form dried particles. Particles were size-selected at 30 nm diameter to overlap with the particles produced via the flow tube and analyzed identically to the flow tube reactor experiments. The resulting acid/base ratio from the atomized particles was assumed to reflect a 1:1 ratio of DMA/HNO_3 based on offline measurements of atomized particle composition.[23] These measurements were used to calibrate the acid/base ratio from the flow tube experiments.

Computational Methods. We explored the potential energy surface of the clusters generated from HNO_3 + DMA using the ABCluster program.[43,44] First, we created 1000 cluster structures and used the PM7 semiempirical method[45] for initial optimization and vibrational frequency calculations. Based on the obtained Gibbs free energies and dipole moments, we separated potential lowest-energy conformers, which were then optimized at the ωB97X-D/6-31+G* level of theory.[46] For 5−10 lowest-energy conformers, the ωB97X-D/6-31++G** level of theory was used for the final optimization and vibrational frequency calculation.[47] We calculated electronic energy corrections on top of the ωB97X-D/6-31++G** structures using the linear-scaling coupled cluster level at the DLPNO−CCSD(T)/aug-cc-pVTZ level of theory with tight PNO criteria.[48,49] Gibbs free energies were calculated at the DLPNO−CCSD(T)/aug-cc-pVTZ//ωB97X-D/6-31++G** level, and the global minimum energy structure for each cluster was identified. All geometries were optimized, vibrational frequencies were calculated using Gaussian16 RevA.03,[50] and electronic energy corrections were performed using Orca version 4.0.1.2.[51]

To study cluster formation kinetics and the dynamics of cluster populations, the calculated Gibbs free energies were used as input in the atmospheric cluster dynamic code (ACDC).[52] Briefly, ACDC calculates the rate coefficients for all collision and evaporation processes within a given set of clusters and vapor molecules and then solves the birth−death equations that describe the dynamics of the cluster population. All the Gibbs free binding energies (in kcal/mol and at 298.15 K) for the minimum energy clusters as well as the structures in the xyz format are available in the Supporting Information. The ACDC code is available from the authors upon request.

■ RESULTS AND DISCUSSION

Size Distributions of Nanoparticles Generated in Dry or Humid Conditions. The number-size distributions of the DMA-HNO_3 particles generated from the flow tube under dry (∼5% RH) and humid (∼55% RH) conditions are shown in Figure 2. In each case, flow rates, reaction time, and gas
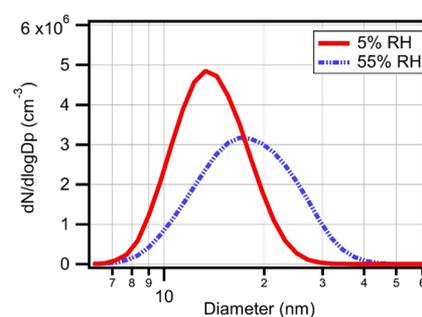
Figure 2. Size distribution of particles generated in dry (5% RH) and humid (55% RH) conditions.

precursor concentrations remained the same; the only difference was in the humidification of N_2. Dimethylamine and nitric acid reacted to form particles readily under dry conditions, and particle sizes ranged from 7 to 30 nm with a volume mean diameter of 16.4 nm. Under humid conditions, water vapor enhanced particle growth, with particle sizes ranging from 7 to 40 nm and the volume mean diameter increasing to 23.6 nm. The total number concentration from the dry to humid case decreased by ∼10%, which has been shown in a previous study to be within error when deriving total number concentration from SMPS data.[53] This suggests that water does not enhance number concentration for these particles despite participating in nanoparticle growth.

While the hygroscopicity of aminium nitrate salts is not well characterized in the literature, ammonium nitrate salts have been studied[54,55] and are observed to have a deliquescence point at 61.5% RH. Aminium sulfate and ammonium sulfate salts have been studied extensively and are found to exhibit different water uptake behaviors.[56−58] While ammonium sulfate deliquesces at ∼79% RH, aminium sulfate salts experience monotonic water uptake.[56] This behavior has been attributed to the possibility that aminium sulfate salts have an amorphous structure in contrast to crystalline ammonium sulfate. In the current study, RH was held at 55%, and HNO_3-DMA nanoparticles experienced growth. If aminium nitrate salts follow the trend of aminium sulfate with respect to their ammonium salt counterparts, it is likely that DMA-HNO_3 particles are amorphous and can uptake water at any RH. However, since SMPS scans were taken continuously with dry air, the size distribution is more reflective of the
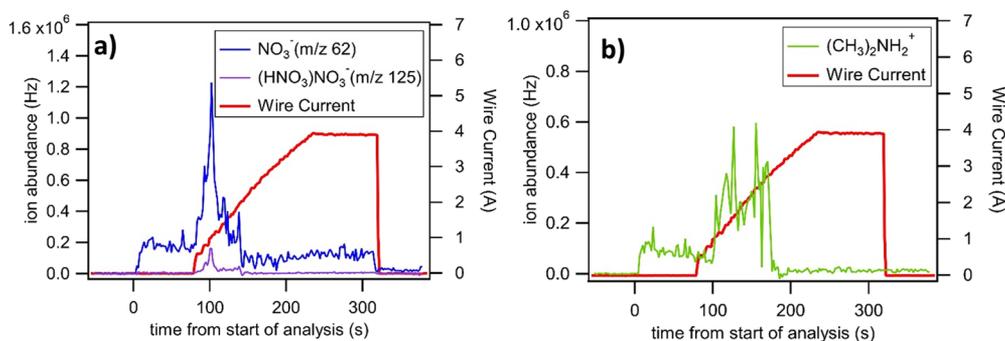
Figure 3. Representative desorption profiles of (a) NO_3^- ion (m/z 62), $HNO_3(NO_3^-)$ ion (m/z 125), and (b) $(CH_3)_2NH_2^+$ ion (m/z 46). Wire current is a proxy for the temperature of the wire.

particle dry diameter in which any water that contributed to growth has been evaporated. The observed growth must be then attributed to enhanced reactive uptake of HNO_3 and DMA into the particle in the presence of water.

Particle formation was stable at constant gas precursor concentrations, and therefore, measured size distributions did not change over time (Figure S4). This allowed for long collection times of the smallest particle sizes for size-resolved studies of nanoparticle composition by TDCIMS.

Desorption Thermograms of HNO_3-DMA Particles under Dry and Humid Conditions. Figure 3 shows representative TDCIMS desorption thermograms of relevant ions detected in this study. Profiles such as these provide qualitative information such as relative volatility and fragmentation pathways; particle adhesion to the metal surface of the collection filament has been shown to generally increase evaporation temperatures of constituents, and this process likely also possesses some chemical specificity.[59,60] Wire desorption temperatures were estimated by applying a power law correlation between the temperature and applied current and are uncertain to ±50 °C. Dimethylaminium ($(CH_3)_2NH_2^+$, m/z 46) and nitrate monomer (NO_3^-, m/z 62) and dimer ($HN_2O_6^-$, m/z 125) ions are detected as soon as the wire enters the heated ion source (40 °C, t = 0 s). At t = 60 s, the wire temperature ramp begins, and desorption is immediately observed for all relevant ions. Nitrate trimer (188 m/z) and water clusters of nitrate and dimethylaminium were not detected or contributed less than 0.1% to their respective total acid and base signal and were not incorporated into acid/base ratio calculations.

Desorption profiles of nitrate and aminium ions in both the dry and humid systems were almost identical, with the only difference being that water cluster peaks of relevant ions appeared during the analysis of humid system particles but contributed to less than 0.5% of the total acid and base signal. The lack of water present in particles formed under humid conditions is most likely caused by the previously mentioned drying effects of the upstream size-selecting nano-DMA as well as the N_2 sheath gas that flows over the collection filament during sampling.

Atomized particles of dimethylamine and nitric acid have been studied for their thermal stability and have been shown to be more stable than ammonium nitrate,[61] with approximately 50% volume fraction remaining at ∼57 °C and complete loss of volume occurring at 77 °C. The thermograms of TDCIMS-detected ions align well with these observations, with desorption occurring as the wire enters the 40 °C ion source (t = 0 s) and with increased desorption occurring immediately

after the TDCIMS wire begins to heat. While the dependence of TDCIMS wire temperature on applied current is not easily characterized due to the complex conditions within the inlet, we estimate the endpoint wire temperature to be approximately 600 °C based on laboratory experiments of the evaporation of different salt samples. Using this information, we estimate the full desorption of particulate nitrate to occur by the time the wire reaches ∼150 °C (t = 145 s, Figure 3a) and of particulate dimethylaminium to occur by ∼250 °C (t = 175 s, Figure 3b). While these temperatures are higher than those reported by Salo et al.,[61] they are consistent with the adsorptive properties of the collection filament discussed above.

Size-Resolved Composition Measurements. In the following discussion, we use the term "neutral" to mean a fully neutralized acid/base ratio (i.e., 1:1 for the system studied here). Our use of this term applies to the relative concentration of particulate acid and base compounds only and should not be extended to particle or bulk solution pH. Figure 4 shows the
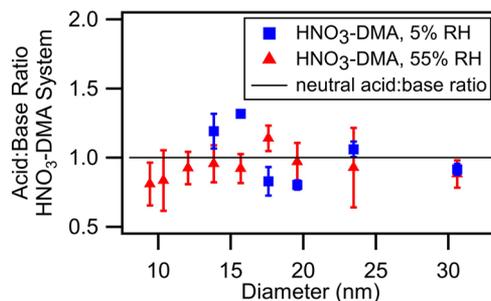
Figure 4. Size-resolved acid/base ratios of HNO_3-DMA particles. Red triangles represent particles formed in dry conditions, while blue squares represent particles formed in humid conditions. The black line is to guide the eye to a neutral 1:1 acid/base ratio.

TDCIMS-measured, size-resolved acid/base ratio of particles formed from nitric acid and dimethylamine in both dry (∼5% RH) and humid (∼55% RH) conditions. The acid/base ratio was calculated by dividing the sum of the ion signals associated with nitrate by the sum of ion signals associated with aminium. This ratio was normalized to the acid/base ratio measured from 30 nm atomized HNO_3-DMA salt particles to account for relative sensitivity of the TDCIMS to nitrate and aminium ions. For the humid system, the shifting of the size distribution to larger sizes (see Figure 2) meant that insufficient sample mass could be collected for particles smaller than 12 nm in diameter. In both the dry and humid cases, the acid/base ratio

does not deviate strongly from a neutral 1:1 ratio of HNO_3/DMA.

While these results confirm the notion that nitric acid and dimethylamine are too volatile to exist in the particle phase without neutralization, Chen et al. found that, in nanoparticles formed from sulfuric acid and ammonia/dimethylamine under both humid and dry conditions, particles smaller than 15 nm in diameter did not have a neutral acid/base ratio.[23] In comparison, for the HNO_3-DMA particles produced in the absence of water, normalized acid/base ratios ranged from 0.81 to 1.14 over the size range of 9−30 nm. In the presence of water, acid/base ratios had a larger spread and ranged from 0.80 to 1.32. In both cases, the particle acid/base ratio did not have distinct trends toward more acidic or more basic particles at any size range. The fact that the measurements of acid/base ratio of HNO_3-DMA particles in this study exhibit trends so close to neutrality suggests fundamental chemical differences between salts of nitrate and those of sulfate. Some of these differences may include sulfuric acid's greater number of hydrogen bonding sites, higher acidity, and lower volatility than those of nitric acid.

To more closely examine the particle growth process, clusters of nitric acid and dimethylamine were modeled to derive the most stable conformations. Results and their interpretation are presented in the next section. While the modeled clusters (max diameter ∼1.5 nm) do not reflect the size regime of the nanoparticle measurements (9−30 nm), they do provide insights into initial growth pathways of these particles that lead to the formation of the nanoparticles that were measured by TDCIMS. Acid−base chemistry is the only possible way for particles to form and grow in this chemical system, and cluster calculations allows us to directly examine molecule-by-molecule addition to clusters.

Cluster Modeling. In this section in which we present modeling results of cluster chemistry, we refer to nitric acid as NA, dimethylamine as D, and water as W. For example, a cluster of two nitric acid molecules, one dimethylamine molecule, and one water molecule will be referred to as 2NA1D1W. For many acid−base systems, the formation of a heterodimer, a cluster with one acid and one base molecule, has been demonstrated to be a crucial step in particle formation.[6,13,62,63] The Gibbs free energy of the reaction that produces the DMA-HNO_3 heterodimer from DMA + HNO_3 is −5.7 kcal/mol at 298.15 K, meaning that the intermolecular interaction between nitric acid and dimethylamine is very weak (compare, for example, the Gibbs free energies of formation of heterodimers of sulfuric acid-dimethylamine (H_2SO_4-DMA) and sulfuric acid-ammonia (H_2SO_4-NH_3), which are −13.5 and −6.8 kcal/mol, respectively). As the calculated structure shown in Figure 5a shows, the reason for the weak interaction between nitric acid and dimethylamine is the absence of proton transfer in the heterodimer. Once the heterodimer is formed, additional cluster growth can occur via the addition of a second dimethylamine or nitric acid molecule, leading to the formation of 1NA2D or 2NA1D clusters. As Figure 5b,c shows, in both clusters, there is proton transfer from nitric acid to dimethylamine. The neutral molecule stabilizes the ion pair by forming hydrogen bonds with the anion and cation. The addition of nitric acid to the heterodimer is more thermodynamically favorable (−4.7 kcal/mol) than the addition of dimethylamine (−1.0 kcal/mol). This can be explained by referring to the cluster structures, which show that the 2NA1D and 1NA2D clusters both form three
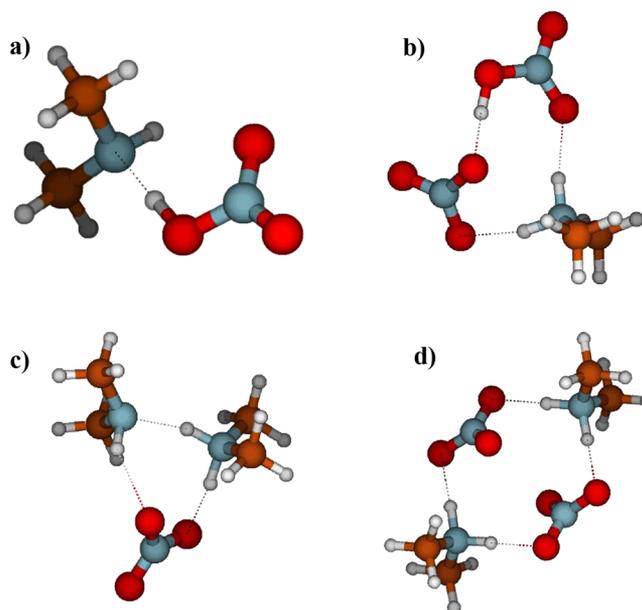

Figure 5. Clusters of (a) 1NA1D, (b) 2NA1D, (c) 1NA2D, and (d) 2NA2D. Color coding: carbon atoms are brown, oxygen atoms are red, nitrogen atoms are blue, and hydrogen atoms are gray. Dotted lines indicate hydrogen bonding between molecules.

hydrogen bonding interactions. However, while the addition of a second dimethylamine molecule provides another hydrogen bond between a nitrogen atom and a hydrogen atom, the addition of a nitric acid molecule results in a stronger hydrogen bond between an oxygen atom and hydrogen atom.

The addition reaction of dimethylamine to the 2NA1D cluster, a neutralization step, is highly favorable with a Gibbs free energy for this reaction of −17.1 kcal/mol. This is because both nitric acid molecules have given their protons to the two dimethylamine molecules and a symmetric cluster is formed (Figure 5d). In each modeled cluster formation step, the addition of nitric acid to the neutral cluster (xNAxD) is thermodynamically more favorable than the addition of dimethylamine. A similar trend is also observed for other acid−base pairs, for instance, sulfuric acid cluster formation with dimethylamine or ammonia.[19] The neutralization steps are highly favorable since the number of proton transfer reactions is maximized, and thus the formed neutral clusters are most stable. It should be noted that, even if the neutralization steps are thermodynamically highly favorable, there is likely to exist a kinetic barrier due to hydrogen-bond breaking and cluster rearrangement as shown in the study by DePalma et al.[64]

We have calculated the evaporation rates for each cluster from the Gibbs free formation energies (see the Supporting Information for details) for both clusters formed with and without water. Figure 6 shows the total evaporation rates of the cluster sizes studied, starting from 1NA1D and ending at 4NA4D, without the presence of water. As mentioned previously, the heterodimer 1NA1D is very weakly bound, which results in an evaporation rate as large as 7×10^5 s^{-1}. This volatility of the heterodimer cluster highlights the necessity for the high concentrations of gas-phase nitric acid and dimethylamine for nucleation to occur. The smallest stable cluster against evaporation is 2NA2D for which the evaporation rate is ∼7 orders of magnitude lower than that of the heterodimer. This dramatic decrease can be attributed
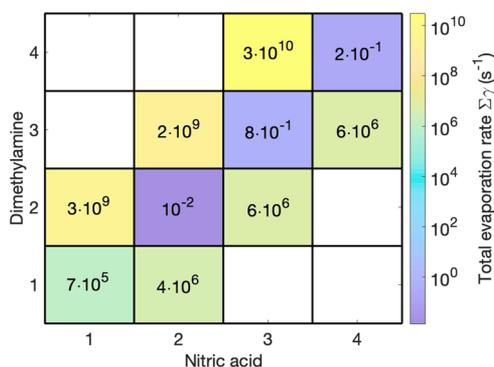
Figure 6. Overall evaporation rates for clusters of 1−4 nitric acid and 1−4 dimethylamine molecules at 298.15 K. Cells are colored from purple (lowest evaporation rates) to yellow (highest evaporation rates).

for proton transfer reactions and cluster symmetry as discussed above. All large neutral clusters are relatively stable against evaporation, meaning that their total evaporation rate, defined as one or more molecules evaporating from the cluster, is smaller than 1 evaporation event per second. The clusters with nonequal numbers of acid and base molecules are unstable since the additional acid or base molecules are likely to evaporate very fast because proton transfer has not occurred. The clusters with compositions of $(x + 1)$NAxD have a ~3 order of magnitude lower evaporation rate than the clusters with a xNA$(x + 1)$D composition, which supports the hypothesis that clusters grow by addition of nitric acid first and then by neutralization by dimethylamine. Due to the significant difference in evaporation rates between neutral and acidic or basic clusters, we can assume that neutral clusters are the most stable ones independent of the particle size. This means that, even though our computational and experimental methods leave a gap between 1 and 8 nm particle diameters, it is a reasonable assumption that particles are neutral also in that size regime.

In addition, we have studied HNO$_3$-DMA clusters containing 1−4 water molecules. In general, water binds very weakly to these clusters and does not improve cluster stability significantly (Figure S4M). The interaction between nitric acid and water is very weak (−0.3 kcal/mol), and between dimethylamine and water, it is even less favorable (0.7 kcal/mol). The Gibbs free formation energy of the 1NA1D1W cluster is −5.9 kcal/mol, meaning that the Gibbs free energy is lowered by 0.2 kcal/mol compared to the 1NA1D cluster. Although the presence of only one water molecule is able to promote the proton transfer from nitric acid to dimethylamine, the cluster is still very weakly bound and thus likely to evaporate. The Gibbs free energy of the addition of second water molecule to the 1NA1D1W cluster is −1.0 kcal/mol, and those of the additions of the third and fourth water molecules are −0.3 and −0.2 kcal/mol, respectively. Since the water molecule addition reactions are thermodynamically only slightly favorable, the evaporation rates of the 1NA1D(1−4)W clusters are on the order of 10^{10} s^{-1}; that is, they have 5 orders of magnitude higher evaporation rates than the dry 1NA1D cluster due to the evaporation of water. Also, in the case of other clusters, water molecules are not capable of interacting with the cluster strongly enough, and indeed, all of the evaporation rates are very high, 10^8−10^{12} s^{-1} (see Figure S4). This implies that the role of hydration in the initial steps

of HNO$_3$-DMA particle formation is negligible, and the main clustering pathway goes via dry nitric acid-dimethylamine cluster formation (as explained above) leading to an acid/base ratio of 1:1 regardless of the level of relative humidity. This result is in excellent agreement with the experimental findings of this study. In addition, it has been previously shown for the H$_2$SO$_4$-DMA system that water has only a minor effect in particle formation,[34] reportedly due to a small number of available hydrogen bonds.[65] Since nitric acid has a lower number of possibilities to form hydrogen bonds than sulfuric acid, it is not surprising that water cannot enhance the formation of HNO$_3$-DMA particles. In the Supporting Information, we have demonstrated that the increased RH does not increase the particle formation rate at any laboratory or atmospherically relevant conditions. This is also apparent in the integrated number concentration for both the dry and humid systems where no significant enhancement of particle number concentration was observed with increased RH. The instability of water molecules in DMA-HNO$_3$ particles suggests that our observations of enhanced particle growth in the presence of water were not necessarily because of water uptake but rather water molecules facilitating the proton transfer reaction between nitric acid and dimethylamine to enhance reactive uptake. However, it is possible that, at sizes larger than a 4NA4D cluster, water may be able to form enough hydrogen bonds to enhance particle growth.

Comparison to Sulfuric Acid-Dimethylamine System. Given that these cluster calculations have provided a reasonable theoretical justification for the observed 1:1 acid/base ratios in DMA-HNO$_3$ nanoparticles, we also calculated the evaporation rates for clusters formed from sulfuric acid and dimethylamine under dry conditions. For this comparison, we refer to sulfuric acid as SA for cluster identification.

The minimum energy structures and Gibbs free energies for clusters containing 0−4 H$_2$SO$_4$ molecules and 0−4 DMA molecules are taken from our previous study.[66] Figure 7 shows
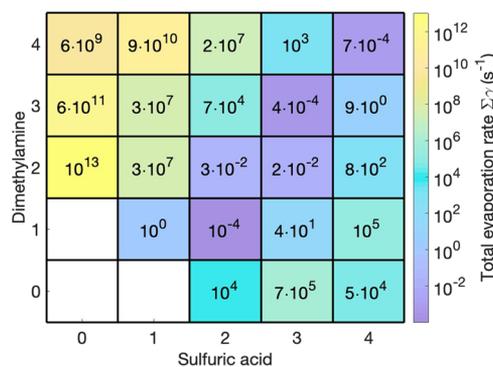

Figure 7. Overall evaporation rates for clusters of 1−4 sulfuric acid and 1−4 dimethylamine molecules at 298.15 K. Cells are colored from purple (lowest evaporation rates) to yellow (highest evaporation rates).

the calculated evaporation rates for H$_2$SO$_4$-DMA clusters. Unlike for HNO$_3$-DMA clusters, in which only the stable clusters occur with an acid/base ratio of 1:1, H$_2$SO$_4$-DMA clusters are stable in both the diagonal axis and below the diagonal; that is, acidic clusters are also stable against evaporation.

The calculated evaporation rate for the 1SA1D heterodimer is over 5 orders of magnitude lower than that of the 1NA1D

heterodimer. The reason for this can be found from the cluster structures shown in Figure 8: in the 1SA1D cluster, sulfuric
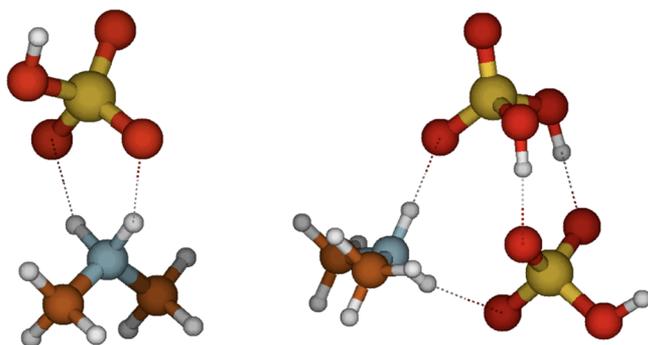
Figure 8. Molecular structures of 1SA1D (left) and 2SA1D (right). Color coding: sulfur atoms are yellow, oxygen atoms are red, nitrogen atoms are blue, and hydrogen atoms are gray. Dotted lines indicate hydrogen bonding interactions.

acid has donated a proton to dimethylamine and there are two intermolecular interactions between the ion pair, while as previously discussed, there is no proton transfer in the 1NA1D cluster and molecules are interacting via one hydrogen bond. As measurements for H_2SO_4-DMA particles have shown, the small sulfuric acid-dimethylamine particles can contain either the same amount of acid and base molecules or more acid than base molecules.[22,23,62] That is likely to be dependent on the conditions in which measurements are performed as well as the technique used to measure composition. These findings help shed light on the experimental results of Chen et al.[23] and Lawler et al.,[22] especially in regard to the observation that the smallest H_2SO_4-DMA nanoparticles tend to be more acidic despite the presence of excess gas-phase base. In the context of this study, the different behaviors of HNO_3-DMA and H_2SO_4-DMA particles can be explained by the strength of intermolecular interactions in the clusters and thus cluster stability. Intermolecular interactions between neutral nitric acid and nitrate or dimethylaminium ions are weak, and thus, more acidic HNO_3-DMA clusters are evaporating with a rate higher than 10^6 s^{-1}. However, in the 2SA1D cluster structure, sulfuric acid binds very strongly (Gibbs free energy is −33.8 kcal/mol) to its deprotonated bisulfate counterpart. Thus, additional sulfuric acid molecules in the H_2SO_4-DMA cluster, in which proton transfer has occurred, are not likely to evaporate. This allows clusters of H_2SO_4-DMA to grow with a larger than 1:1 acid/base ratio.

CONCLUSIONS

In this study, we performed size-resolved measurements of particles formed from dimethylamine and nitric acid under dry and humid conditions. Number-size distributions of these particles indicate that particles grow larger with higher relative humidity, most likely due to enhanced reactive uptake of HNO_3 and DMA. Within experimental uncertainty, the acid/base ratio for nanoparticles formed under both dry and humid conditions remains at unity throughout growth from 9 to 30 nm in diameter. Modeled cluster evaporation rates show that clusters are only stable when a 1:1 HNO_3/DMA ratio occurs, with and without added water vapor. This behavior is in agreement with a theoretical picture of proton exchange between a Brønsted−Lowry acid (HNO_3) and base (NH_3), forming a salt with a 1:1 acid/base ratio. Cluster calculations

and experimental results confirm what the chemical theory might suggest: volatile precursors such as nitric acid and dimethylamine can only contribute to nanoparticle growth through the formation of nonvolatile salts. In contrast, calculations performed on clusters formed from precursors containing one nonvolatile component, sulfuric acid, show that nanoparticles formed from this system will likely deviate from neutrality due to the increased likelihood of stable structures involving both the deprotonated and neutral sulfuric acid molecule. While the current study provides insights into reactive uptake of acids and bases into nanoparticles, it is clear that each chemical system exhibits unique properties that require in depth experimental and theoretical studies. Future research should focus on elucidating trends between acid and base structures (e.g., number of hydrogen bond donors or acceptors, symmetry, and shape) and nanoparticle composition below 15 nm in diameter.

ASSOCIATED CONTENT

Ⓢ Supporting Information
The Supporting Information is available free of charge on the ACS Publications website at DOI: 10.1021/acs.jpca.9b03326.

> Dimethylamine gas-phase measurements, variability attributed to integration windows in TDCIMS data processing, TDCIMS data linearity tests, particle size distribution stability, computational methods equations, hydrated HNO_3-DMA cluster evaporation rates, and Gibbs free binding energies for each cluster reported (PDF)

AUTHOR INFORMATION

Corresponding Author
*E-mail: jimsmith@uci.edu.
ORCID Ⓞ
Nanna Myllys: 0000-0003-0384-7277
Kelley C. Barsanti: 0000-0002-6065-8643
Bryan M. Wong: 0000-0002-3477-8043
James N. Smith: 0000-0003-4677-8224

Notes
The authors declare no competing financial interest.

ACKNOWLEDGMENTS

REFERENCES

(1) Kuang, C.; McMurry, P. H.; McCormick, A. V. Determination of Cloud Condensation Nuclei Production from Measured New Particle Formation Events. *Geophys. Res. Lett.* **2009**, *36*, L09822.
(2) Zhang, R.; Khalizov, A.; Wang, L.; Hu, M.; Xu, W. Nucleation and Growth of Nanoparticles in the Atmosphere. *Chem. Rev.* **2012**, *112*, 1957−2011.
(3) Finlayson-Pitts, B. J.; Pitts, J. N., Jr. *Chemistry of the Upper and Lower Atmosphere*; Academic Press: 2000.
(4) Chan, T. W.; Mozurkewich, M. Measurement of the Coagulation Rate Constant for Sulfuric Acid Particles as a Function of Particle Size

Using Tandem Differential Mobility Analysis. *J. Aerosol Sci.* **2001**, *32*, 321−339.

(5) Schobesberger, S.; Franchin, A.; Bianchi, F.; Rondo, L.; Duplissy, J.; Kürten, A.; Ortega, I. K.; Metzger, A.; Schnitzhofer, R.; Almeida, J.; et al. On the Composition of Ammonia−sulfuric-Acid Ion Clusters during Aerosol Particle Formation. *Atmos. Chem. Phys.* **2015**, *15*, 55−78.

(6) Elm, J. Elucidating the Limiting Steps in Sulfuric Acid-Base New Particle Formation. *J. Phys. Chem. A* **2017**, *121*, 8288−8295.

(7) Zollner, J. H.; Glasoe, W. A.; Panta, B.; Carlson, K. K.; McMurry, P. H.; Hanson, D. R. Sulfuric Acid Nucleation: Power Dependencies, Variation with Relative Humidity, and Effect of Bases. *Atmos. Chem. Phys.* **2012**, *12*, 4399−4411.

(8) Bzdek, B. R.; Zordan, C. A.; Pennington, M. R.; Luther, G. W., III; Johnston, M. V. Quantitative Assessment of the Sulfuric Acid Contribution to New Particle Growth. *Environ. Sci. Technol.* **2012**, *46*, 4365−4373.

(9) Sipilä, M.; Berndt, T.; Petäjä, T.; Brus, D.; Vanhanen, J.; Stratmann, F.; Patokoski, J.; Mauldin, R. L., III; Hyvärinen, A.-P.; Lihavainen, H.; et al. The Role of Sulfuric Acid in Atmospheric Nucleation. *Science* **2010**, *327*, 1243−1246.

(10) Weber, R. J.; McMurry, P. H.; Eisele, F. L.; Tanner, D. J. Measurement of Expected Nucleation Precursor Species and 3−500-Nm Diameter Particles at Mauna Loa Observatory, Hawaii. *J. Atmos. Sci.* **1995**, *52*, 2242−2257.

(11) Kuang, C.; McMurry, P. H.; McCormick, A. V.; Eisele, F. L. Dependence of Nucleation Rates on Sulfuric Acid Vapor Concentration in Diverse Atmospheric Locations. *J. Geophys. Res. : Atmos.* **2008**, *113*, D10209.

(12) Kirkby, J.; Curtius, J.; Almeida, J.; Dunne, E.; Duplissy, J.; Ehrhart, S.; Franchin, A.; Gagné, S.; Ickes, L.; Kürten, A.; et al. Role of Sulphuric Acid, Ammonia and Galactic Cosmic Rays in Atmospheric Aerosol Nucleation. *Nature* **2011**, *476*, 429−433.

(13) Almeida, J.; Schobesberger, S.; Kürten, A.; Ortega, I. K.; Kupiainen-Määttä, O.; Praplan, A. P.; Adamov, A.; Amorim, A.; Bianchi, F.; Breitenlechner, M.; et al. Molecular Understanding of Sulphuric Acid−amine Particle Nucleation in the Atmosphere. *Nature* **2013**, *502*, 359−363.

(14) Weber, R. J.; Marti, J. J.; McMurry, P. H.; Eisele, F. L.; Tanner, D. J.; Jefferson, A. Measured Atmospheric New Particle Formation Rates: Implications for Nucleation Mechanisms. *Chem. Eng. Commun.* **2007**, *151*, 53−64.

(15) Smith, J. N.; Dunn, M. J.; VanReken, T. M.; Iida, K.; Stolzenburg, M. R.; McMurry, P. H.; Huey, L. G. Chemical Composition of Atmospheric Nanoparticles Formed from Nucleation in Tecamac, Mexico: Evidence for an Important Role for Organic Species in Nanoparticle Growth. *Geophys. Res. Lett.* **2008**, *35*, L04808.

(16) Smith, J. N.; Barsanti, K. C.; Friedli, H. R.; Ehn, M.; Kulmala, M.; Collins, D. R.; Scheckman, J. H.; Williams, B. J.; Mcmurry, P. H. Observations of Aminium Salts in Atmospheric Nanoparticles and Possible Climatic Implications. *Proc. Natl. Acad. Sci. U. S. A.* **2010**, 6634.

(17) Lawler, M. J.; Whitehead, J.; O'Dowd, C.; Monahan, C.; McFiggans, G.; Smith, J. N. Composition of 15−85 Nm Particles in Marine Air. *Atmos. Chem. Phys.* **2014**, *14*, 11557−11569.

(18) Barsanti, K. C.; McMurry, P. H.; Smith, J. N. The Potential Contribution of Organic Salts to New Particle Growth. *Atmos. Chem. Phys.* **2009**, *9*, 2949−2957.

(19) Bzdek, B. R.; DePalma, J. W.; Johnston, M. V. Mechanisms of Atmospherically Relevant Cluster Growth. *Acc. Chem. Res.* **2017**, *50*, 1965−1975.

(20) Schobesberger, S.; Junninen, H.; Bianchi, F.; Lönn, G.; Ehn, M.; Lehtipalo, K.; Dommen, J.; Ehrhart, S.; Ortega, I. K.; Franchin, A.; et al. Molecular Understanding of Atmospheric Particle Formation from Sulfuric Acid and Large Oxidized Organic Molecules. *Proc. Natl. Acad. Sci. U. S. A.* **2013**, *110*, 17223−17228.

(21) Kim, J.; Ahlm, L.; Yli-Juuti, T.; Lawler, M.; Keskinen, H.; Tröstl, J.; Schobesberger, S.; Duplissy, J.; Amorim, A.; Bianchi, F.; et al. Hygroscopicity of Nanoparticles Produced from Homogeneous Nucleation in the CLOUD Experiments. *Atmos. Chem. Phys.* **2016**, *16*, 293−304.

(22) Lawler, M. J.; Winkler, P. M.; Kim, J.; Ahlm, L.; Tröstl, J.; Praplan, A. P.; Schobesberger, S.; Kürten, A.; Kirkby, J.; Bianchi, F.; et al. Unexpectedly Acidic Nanoparticles Formed in Dimethylamine−ammonia−sulfuric-Acid Nucleation Experiments at CLOUD. *Atmos. Chem. Phys.* **2016**, *16*, 13601−13618.

(23) Chen, H.; Chee, S.; Lawler, M. J.; Barsanti, K. C.; Wong, B. M.; Smith, J. N. Size Resolved Chemical Composition of Nanoparticles from Reactions of Sulfuric Acid with Ammonia and Dimethylamine. *Aerosol Sci. Technol.* **2018**, *52*, 1120−1133.

(24) Appel, B. R.; Wall, S. M.; Tokiwa, Y.; Haik, M. Simultaneous Nitric Acid, Particulate Nitrate, and Acidity Measurements in Ambient Air. *Atmos. Environ.* **1980**, *14*, 549−554.

(25) Huang, G.; Zhou, X.; Deng, G.; Qiao, H.; Civerolo, K. Measurements of Atmospheric Nitrous Acid and Nitric Acid. *Atmos. Environ.* **2002**, *36*, 2225−2235.

(26) Cass, G. R.; Hughes, L. A.; Bhave, P.; Kleeman, M. J.; Allen, J. O.; Salmon, L. G. The Chemical Composition of Atmospheric Ultrafine Particles. *Philos. Trans. R. Soc. London, Ser. A* **2000**, *358*, 2581−2592.

(27) Pakkanen, T. A. Study of Formation of Coarse Particle Nitrate Aerosol. *Atmos. Environ.* **1996**, *30*, 2475−2482.

(28) Noble, C. A.; Prather, K. A. Real-Time Measurement of Correlated Size and Composition Profiles of Individual Atmospheric Aerosol Particles. *Environ. Sci. Technol.* **1996**, *30*, 2667−2680.

(29) Smith, J. N.; Moore, K. F.; Mcmurry, P. H.; Eisele, F. L. Atmospheric Measurements of Sub-20 Nm Diameter Particle Chemical Composition by Thermal Desorption Chemical Ionization Mass Spectrometry. *Aerosol Sci. Technol.* **2004**, *38*, 100−110.

(30) Tröstl, J.; Chuang, W. K.; Gordon, H.; Heinritzi, M.; Yan, C.; Molteni, U.; Ahlm, L.; Frege, C.; Bianchi, F.; Wagner, R.; et al. The Role of Low-Volatility Organic Compounds in Initial Particle Growth in the Atmosphere. *Nature* **2016**, *533*, 527−531.

(31) Cheng, C.; Huang, Z.; Chan, C. K.; Chu, Y.; Li, M.; Zhang, T.; Ou, Y.; Chen, D.; Cheng, P.; Li, L.; Gao, W.; Huang, Z.; Huang, B.; Fu, Z.; Zhou, Z. Characteristics and Mixing State of Amine-Containing Particles at a Rural Site in the Pearl River Delta, China. *Atmos. Chem. Phys.* **2018**, *18*, 9147−9159.

(32) Chan, L. P.; Chan, C. K. Role of the Aerosol Phase State in Ammonia/Amines Exchange Reactions. *Environ. Sci. Technol.* **2013**, *47*, 5755−5762.

(33) Chen, H.; Finlayson-Pitts, B. J. New Particle Formation from Methanesulfonic Acid and Amines/Ammonia as a Function of Temperature. *Environ. Sci. Technol.* **2016**, *51*, 243−252.

(34) Olenius, T.; Halonen, R.; Kurtén, T.; Henschel, H.; Kupiainen-Määttä, O.; Ortega, I. K.; Jen, C. N.; Vehkamäki, H.; Riipinen, I. New Particle Formation from Sulfuric Acid and Amines: Comparison of Monomethylamine, Dimethylamine, and Trimethylamine. *J. Geophys. Res.: Atmos.* **2017**, *122*, 7103−7118.

(35) Bzdek, B. R.; Ridge, D. P.; Johnston, M. V. Size-Dependent Reactions of Ammonium Bisulfate Clusters with Dimethylamine. *J. Phys. Chem. A* **2010**, *114*, 11638−11644.

(36) Berndt, T.; Sipilä, M.; Stratmann, F.; Petäjä, T.; Vanhanen, J.; Mikkilä, J.; Patokoski, J.; Taipale, R.; Mauldin, R. L., III; Kulmala, M. Enhancement of Atmospheric H_2SO_4/H_2O Nucleation: Organic Oxidation Products versus Amines. *Atmos. Chem. Phys.* **2013**, *13*, 16301−16335.

(37) Bzdek, B. R.; Ridge, D. P.; Johnston, M. V. Amine Exchange into Ammonium Bisulfate and Ammonium Nitrate Nuclei. *Atmos. Chem. Phys.* **2010**, *10*, 3495−3503.

(38) Murphy, S. M.; Sorooshian, A.; Kroll, J. H.; Ng, N. L.; Chhabra, P.; Tong, C.; Surratt, J. D.; Knipping, E.; Flagan, R. C.; Seinfeld, J. H. Secondary Aerosol Formation from Atmospheric Reactions of Aliphatic Amines. *Atmos. Chem. Phys.* **2007**, *7*, 2313−2337.

(39) Sareen, N.; Waxman, E. M.; Turpin, B. J.; Volkamer, R.; Carlton, A. G. Potential of Aerosol Liquid Water to Facilitate Organic Aerosol Formation: Assessing Knowledge Gaps about Precursors and Partitioning. *Environ. Sci. Technol.* **2017**, *51*, 3327−3335.

(40) Voisin, D.; Smith, J. N.; Sakurai, H.; Mcmurry, P. H.; Eisele, F. L. Thermal Desorption Chemical Ionization Mass Spectrometer for Ultrafine Particle Chemical Composition. *Aerosol Sci. Technol.* **2003**, *37*, 471−475.

(41) Chen, D.-R.; Pui, D. Y. H. A High Efficiency, High Throughput Unipolar Aerosol Charger for Nanoparticles. *J. Nanopart. Res.* **1999**, *1*, 115−126.

(42) McMurry, P. H.; Ghimire, A.; Ahn, H.-K.; Sakurai, H.; Moore, K.; Stolzenburg, M.; Smith, J. N. Sampling Nanoparticles for Chemical Analysis by Low Resolution Electrical Mobility Classification. *Environ. Sci. Technol.* **2009**, *43*, 4653−4658.

(43) Zhang, J.; Dolg, M. ABCluster: The Artificial Bee Colony Algorithm for Cluster Global Optimization. *Phys. Chem. Chem. Phys.* **2015**, *17*, 24173−24181.

(44) Zhang, J.; Dolg, M. Global Optimization of Clusters of Rigid Molecules Using the Artificial Bee Colony Algorithm. *Phys. Chem. Chem. Phys.* **2016**, *18*, 3003−3010.

(45) Stewart, J. J. P. Optimization of Parameters for Semiempirical Methods V: Modification of NDDO Approximations and Application to 70 Elements. *J. Mol. Model.* **2007**, *13*, 1173−1213.

(46) Chai, J.-D.; Head-Gordon, M. Long-Range Corrected Hybrid Density Functionals with Damped Atom − Atom Dispersion Corrections. *Phys. Chem. Chem. Phys.* **2008**, *10*, 6615−6620.

(47) Myllys, N.; Elm, J.; Kurtén, T. Density Functional Theory Basis Set Convergence of Sulfuric Acid-Containing Molecular Clusters. *Comput. Theor. Chem.* **2016**, *1098*, 1−12.

(48) Riplinger, C.; Pinski, P.; Becker, U.; Valeev, E. F.; Neese, F. Sparse Maps — A Systematic Infrastructure for Reduced-Scaling Electronic Structure Methods. II. Linear Scaling Domain Based Pair Natural Orbital Coupled Cluster Theory. *J. Chem. Phys.* **2016**, *144*, No. 024109.

(49) Myllys, N.; Elm, J.; Halonen, R.; Kurtén, T.; Vehkamäki, H. Coupled Cluster Evaluation of the Stability of Atmospheric Acid−Base Clusters with up to 10 Molecules. *J. Phys. Chem. A* **2016**, *120*, 621−630.

(50) Frisch, M. J.; Trucks, G. W.; Schlegel, H. B.; Scuseria, G. E.; Robb, M. A.; Cheeseman, J. R.; Scalmani, G.; Barone, V.; Petersson, G. A.; Nakatsuji, H.;et al.. *Gaussian16* Revision A.03. Gaussian, Inc.: 2016.

(51) Neese, F. The ORCA Program System. *WIREs Comput. Mol. Sci.* **2012**, *2*, 73−78.

(52) McGrath, M. J.; Olenius, T.; Ortega, I. K.; Loukonen, V.; Paasonen, P.; Kurtén, T.; Kulmala, M.; Vehkamäki, H. Atmospheric Cluster Dynamics Code: A Flexible Method for Solution of the Birth-Death Equations. *Atmos. Chem. Phys.* **2012**, *12*, 2345−2355.

(53) Liu, P. S. K.; Deshler, T. Causes of Concentration Differences Between a Scanning Mobility Particle Sizer and a Condensation Particle Counter. *Aerosol Sci. Technol.* **2003**, *37*, 916−923.

(54) Lightstone, J. M.; Onasch, T. B.; Imre, D.; Oatis, S. Deliquescence, Efflorescence, and Water Activity in Ammonium Nitrate and Mixed Ammonium Nitrate/Succinic Acid Microparticles. *J. Phys. Chem. A* **2000**, *104*, 9337−9346.

(55) Hu, D.; Chen, J.; Ye, X.; Li, L.; Yang, X. Hygroscopicity and Evaporation of Ammonium Chloride and Ammonium Nitrate: Relative Humidity and Size Effects on the Growth Factor. *Atmos. Environ.* **2011**, *45*, 2349−2355.

(56) Qiu, C.; Zhang, R. Physiochemical Properties of Alkylaminium Sulfates: Hygroscopicity, Thermostability, and Density. *Environ. Sci. Technol.* **2012**, *46*, 4474−4480.

(57) Braban, C. F.; Abbatt, J. P. D.; Cziczo, D. J. Deliquescence of Ammonium Sulfate Particles at Sub-Eutectic Temperatures. *Geophys. Res. Lett.* **2001**, *28*, 3879−3882.

(58) Walker, J. S.; Wills, J. B.; Reid, J. P.; Wang, L.; Topping, D. O.; Butler, J. R.; Zhang, Y.-H. Direct Comparison of the Hygroscopic Properties of Ammonium Sulfate and Sodium Chloride Aerosol at Relative Humidities Approaching Saturation. *J. Phys. Chem. A* **2010**, *114*, 12682−12691.

(59) Smith, J. N.; Rathbone, G. J. Carboxylic Acid Characterization in Nanoparticles by Thermal Desorption Chemical Ionization Mass Spectrometry. *Int. J. Mass Spectrom.* **2008**, *274*, 8−13.

(60) Chattopadhyay, S.; Ziemann, P. J. Vapor Pressures of Substituted and Unsubstituted Monocarboxylic and Dicarboxylic Acids Measured Using an Improved Thermal Desorption Particle Beam Mass Spectrometry Method. *Aerosol Sci. Technol.* **2005**, 1085.

(61) Salo, K.; Westerlund, J.; Andersson, P. U.; Nielsen, C.; D'Anna, B.; Hallquist, M. Thermal Characterization of Aminium Nitrate Nanoparticles. *J. Phys. Chem. A* **2011**, *115*, 11671−11677.

(62) Kürten, A.; Jokinen, T.; Simon, M.; Sipilä, M.; Sarnela, N.; Junninen, H.; Adamov, A.; Almeida, J.; Amorim, A.; Bianchi, F.; et al. Neutral Molecular Cluster Formation of Sulfuric Acid−Dimethylamine Observed in Real Time under Atmospheric Conditions. *Proc. Natl. Acad. Sci. U. S. A.* **2014**, *111*, 15019−15024.

(63) Petäjä, T.; Sipilä, M.; Paasonen, P.; Nieminen, T.; Kurtén, T.; Ortega, I. K.; Stratmann, F.; Vehkamäki, H.; Berndt, T.; Kulmala, M. Experimental Observation of Strongly Bound Dimers of Sulfuric Acid : Application to Nucleation in the Atmosphere. *Phys. Rev. Lett.* **2011**, *106*, 228302.

(64) DePalma, J. W.; Bzdek, B. R.; Doren, D. J.; Johnston, M. V. Structure and Energetics of Nanometer Size Clusters of Sulfuric Acid with Ammonia and Dimethylamine. *J. Phys. Chem. A* **2012**, *116*, 1030−1040.

(65) Yang, Y.; Waller, S. E.; Kreinbihl, J. J.; Johnson, C. J. Direct Link between Structure and Hydration in Ammonium and Aminium Bisulfate Clusters Implicated in Atmospheric New Particle Formation. *J. Phys. Chem. Lett.* **2018**, *9*, 5647−5652.

(66) Myllys, N.; Chee, S.; Olenius, T.; Lawler, M.; Smith, J. Molecular-Level Understanding of Synergistic Effects in Sulfuric Acid − Amine − Ammonia Mixed Clusters. *J. Phys. Chem. A* **2019**, *123*, 2420−2425.